Performance of Photo-Sensors for KM3NeT

Q. Dorosti Hasankiadeh[a,*], O. Kavatsyuk[a], H. Löhner[a], H. Peek[b], J. Steijger[b],
on behalf of the KM3NeT Consortium

[a] *KVI, University of Groningen, Zernikelaan 25, NL-9747 AA Groningen, The Netherlands*
[b] *Nikhef, Science Park 105, 1098 XG Amsterdam, The Netherlands*

Abstract

The future deep-sea neutrino telescope of multi cubic-km size, KM3NeT, has been designed for an efficient search for high energy neutrinos originating from galactic and extragalactic sources. The detection principle relies on the measurement of Cherenkov light emitted from relativistic charged secondary particles caused by the interaction of neutrinos with matter inside or surrounding the active detection volume. In order to provide a homogeneous photon acceptance and to reduce the environmental background by local coincidences between neighbouring photo sensors, a Digital Optical Module (DOM) containing an array of 31 3-inch diameter photomultiplier tubes (PMTs) has been designed. Optimum performance requires sensitivity to single-photo electrons, high collection efficiency at low dark noise, homogeneous photo-cathode response and excellent timing properties. We have studied the response to single photo electrons of a newly developed 3-inch diameter PMT from ET Enterprises Ltd. A 2D-scanning system with a picosecond laser illuminating various positions on the photo-cathode surface was employed to study the timing and homogeneity of the PMT. Results of these investigations indicate good photo-cathode homogeneity, low dark noise on the sub-kHz level, and an average transit-time spread below 2 ns. Simulations indicate a significantly improved signal-to-background ratio in the multi-PMT DOM as compared to a triplet of optical modules each housing a single 10-inch PMT.

Keywords: KM3NeT, neutrino telescope, optical module, photomultiplier tube
PACS: 95.55.Vj

1. Introduction

The future deep-sea neutrino telescope of multi cubic-km size, KM3NeT [1], has been designed for an efficient search for high energy neutrinos originating from galactic and extragalactic sources. The detection of cosmic neutrinos may provide us with yet concealed information about non-thermal processes in the Universe. Based on the experience of the pilot projects ANTARES [2], NEMO [3] and NESTOR [4] the KM3NeT consortium plans to equip an active detection volume at the bottom of the Mediterranean Sea with an array of digital optical modules (DOMs), i.e. only digital information will be sent from a DOM to shore for further analysis. The detection principle relies on the measurement of Cherenkov light emitted from secondary relativistic charged particles caused by the interaction of neutrinos with matter inside or surrounding the active detection volume. Muon neutrinos may create muon tracks through charged-current interactions, while neutral-current neutrino interactions cause hadronic showers and provide sensitivity to all neutrino flavours. The direction and energy of neutrinos can be inferred from a precise determination of DOM position, arrival time and total detected charge. For the identification of point-like neutrino sources an angular resolution better than 0.3° can be provided for neutrino energies above 10 TeV.

In addition to Cherenkov photons originating from charged tracks or hadronic showers caused by neutrinos, a DOM is exposed to a random optical background which is due to the decay of radioactive isotopes and biological processes in sea water. In ANTARES, each photo sensor of 10-inch diameter measures typically a pulse rate of 60 - 100 kHz, mostly single photo electrons produced by ^{40}K decay (≈40 kHz) and by the bioluminescence from the deep-sea fauna causing a constant contribution with occasional bursts of much higher intensity. These uncorrelated signals are suppressed by requiring local coincidences in nearby photo sensors on each floor of the detector array and a certain minimum number of photon hits on several floors. In order to improve the local optical-background rejection, a multi-PMT DOM (Fig. 1) housing 31 3-inch PMTs has been developed and proposed in the KM3NeT Technical Design Report [5]. The multi-PMT DOM has a number of advantages compared to an optical module (OM) housing a single large PMT, such as a smaller transit time spread, a longer life time, and a better two-photon separation [6] in addition to a simplified charge determination by counting the number of fired PMTs. Small PMTs do not require magnetic shielding, since they are much less sensitive to the Earth's magnetic field. Moreover a multi-PMT DOM has a higher reliability compared to a single-PMT OM, since failure of one small PMT has a limited effect on its total performance. The use of multi-PMT DOMs will significantly improve the reconstruction of neutrino events in KM3NeT. In section 3.4 the expected performance of a multi-

*Corresponding author
Email address: q.dorosti.hasankiadeh@rug.nl (Q. Dorosti Hasankiadeh)

Figure 1: Prototype of the multi-PMT DOM with 31 3-inch PMTs arranged in a 17-inch diameter pressure glass sphere. Insert top right: the photograph of the ET Enterprises Ltd. D783FL 3-inch diameter PMT.

PMT DOM in the presence of optical background is addressed.

2. Instrumentation

2.1. Tested samples

Based on the successful use of 17-inch diameter glass pressure spheres in ANTARES, an optimised geometrical layout of 31 3-inch diameter PMTs has been developed within this envelope. This spatial distribution of PMTs maximises photocathode homogeneity over the range of Cherenkov photon arrival directions. According to the design criteria [5] established for the KM3NeT application, ET Enterprises Ltd. (ETEL) has developed a new type of 3-inch diameter PMT, model D783FL (Fig. 1, the top right picture). The D783FL PMT has a length of about 10 cm with a curved photo cathode and a photo-cathode window matching the curvature of the 17-inch diameter glass sphere of the DOM. The 10-stage linear-box electron multiplier provides a fast timing response. The main characteristics of the D783FL PMT are summarised in Table 1.

Table 1: Characteristics of the D783FL PMT.

Window material	borosilicate
Photocathode	green-enhanced bialkali
Multiplier structure	10-stage-linear box
Quantum efficiency	
at 470 nm	> 20%
at 404 nm	> 32%

2.2. Test bench

Several performance parameters of a number of ETEL PMT prototypes have been studied, such as gain, dark-noise rate, relative collection efficiency, timing characteristics, and afterpulse probability. The individual PMTs were installed inside a light-tight box (dark box) in front of a multi-mode quartz optical fiber guiding light from an external light source to the entrance window of the PMT. The applied external light source is a picosecond laser [7] with wavelength $\lambda = 405$ nm and a time jitter between trigger and pulse of less than 70 ps. In order to

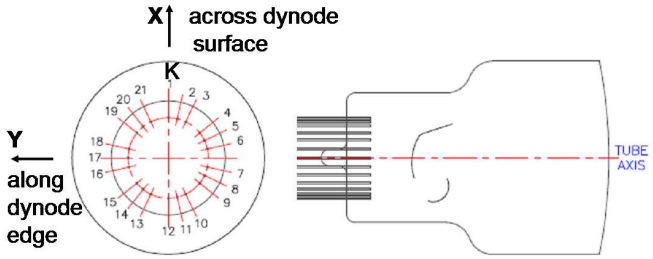

Figure 2: Orientation of the PMT in the measurement setup. The X-axis is defined along the dynode edge and the Y-axis runs across the dynode surface.

attenuate the laser light to the single photo-electron level, we applied a variable neutral density filter. The light was shone perpendicularly to the window of the PMT with a spot diameter of 1.4 mm at the centre of the window. In order to study the homogeneity of the photo-cathode sensitivity, we employed a remotely controlled 2D-scanning system which consists of two linear stages. The stages, equipped with stepper motors with a position precision of 1.5 μm, allow scanning in horizontal and vertical directions. As shown in Fig. 2, we oriented the PMTs such that the horizontal direction (X) was aligned along the dynode edge and the vertical direction (Y) was crossing the dynode surface. The centre of the PMT window is defined as the origin of the coordinate system. The PMT performance was compared at different values of supply voltage, one value providing the nominal gain, at the nominal voltage according to manufacture specification, of about 6×10^6 and the others providing either a 10 times lower or 10 times higher gain. PMT signals were read out with a custom low noise, low heat dissipation amplifier developed for the Multi-PMT DOM at NIKHEF. The current-voltage amplifier has a gain factor of 155 V/A with respect to a load resistor of 50 Ω, and is adapted to the 10 dynode PMTs that can be fitted inside the 17-inch sphere. The amplifier output signals are sampled by a fast sampling Acqiris system [8] with a sampling rate of 8 GHz and input impedance of 50 Ω.

3. Results and Discussion

3.1. Gain and dark-noise rate measurements

The gain of the PMTs was derived from the measured charge spectrum. Figure 3 shows a typical charge spectrum revealing the electronic noise and the single (SPE) and double photoelectron peaks. The peaks are fitted by the sum of two Gaussians. The electronic noise can be separated by a threshold at 0.3 SPE. The *gain* of the PMT can be determined as follows:

$$gain = \frac{SPE[pC]}{e[pC] \times 155} \quad (1)$$

where e is the charge of the electron and 155 is the preamplification factor. Figure 4 shows the gain as function of the applied voltages for five PMT samples. A fairly linear be-

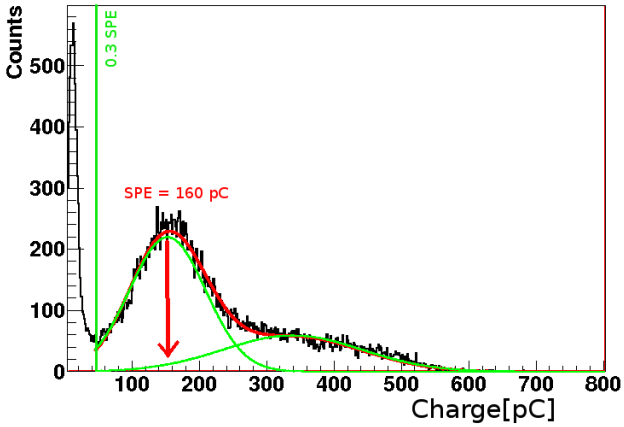

Figure 3: Typical charge spectrum measured at a PMT gain of 6.4×10^6 with a pre-amplification factor 155. The peaks are fitted by the sum of two Gaussians. The positions of the single photo-electron peak (SPE) and the threshold at 0.3 SPE are marked.

haviour is observed with rather similar slope parameters of gain versus supply voltage (HV) defined as

$$slope = \frac{\Delta log(gain)}{\Delta log(HV[V])} \quad (2)$$

To determine the dark-noise rate, we applied a 10 kHz random trigger and measured the charge spectrum without laser light after the PMT was kept for one day in the dark box. We searched for dark pulses in time windows of 20 μs. The dark-noise rate was determined by analysing typically 60k events, counting the number of hits with an amplitude above the noise level of 0.3 SPE, and dividing by the dead-time corrected measurement time. The determined dark-noise rates for 5 PMT prototypes are summarised in Table 2 containing values measured at a temperature of 22 ± 1° C. The dark rates are expected to decrease by about a factor 2 at the average deep-sea temperature of 13.6°C. Table 2 compiles results of measurements at two different gains of other performance parameters such as peak-to-valley ratio (P/V, with laser at SPE intensity and without laser), transit time spread (σ) at the centre of PMTs, and after-pulse probabilities in a 400 ns time window. The typical after-pulse probability in a 3 μs time window is 6% and considered satisafctory.

3.2. Photo-cathode homogeneity

The photo-cathode surfaces of several PMTs were scanned by shining laser light with a spot diameter of 1.4 mm on various positions of the entrance window across the X and Y directions (Fig. 2). For every position we measured the collected charge by integrating the charge spectrum above the 0.3 SPE threshold. Figure 5 shows a typical distribution of the measured relative collection efficiency as a function of position on the PMT entrance window. The measured charge values at various positions are normalised to the charge value at the centre of the photo cathode (:= 100% collection efficiency). The vertical lines in Fig. 5 indicate the effective photo-cathode range, defined as the range of radii where the relative collection efficiency stays above 90% relative to that at the centre (marked

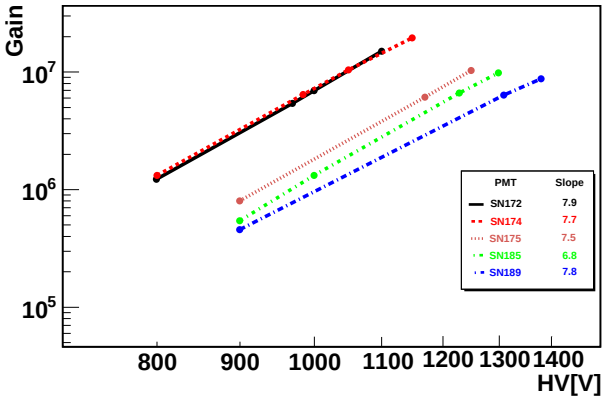

Figure 4: Gain as function of the applied voltage for 5 PMT samples. The data points on the double-log scale are fitted by a linear function. The slope is determined by equation 2.

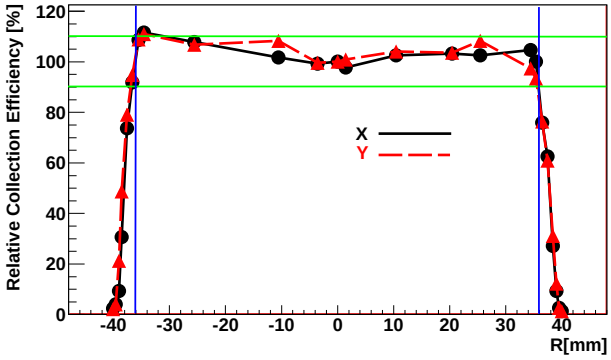

Figure 5: Typical measured relative collection efficiency as a function of the positions on the photo cathode. We scanned the PMT in the X (black solid line with circle markers) and the Y (red (gray) dashed line with triangle markers) directions, as defined in Fig. 2. The horizontal lines indicate the range where the collection efficiency remains within ±10% from that at the centre, and the vertical lines mark the effective photo-cathode area.

by the lower horizontal line). The obtained data on the relative collection efficiency for a number of D783FL PMTs result in an effective photo-cathode radius of 36 ± 0.4 mm. The uncertainty is estimated from the quadratic sum of the approximately Gaussian laser-spot width and the error in determining the slope of the collection efficiency at the photo-cathode edge.

3.3. Timing characteristics

For every scanned position we also recorded the time-after-laser-trigger and from the corresponding distributions for each position we deduced the standard deviation σ. Typical measured values of $\sigma[ns]$ as a function of the position on the PMT entrance window at the gain of 5×10^6 are shown in Fig. 6. The vertical lines mark the effective photo-cathode area. The obtained data indicate that the transit time spread (TTS) fairly lies below 2 ns except the region near the edge of the effective photo-cathode area. Outside this region the TTS appears to decrease which is due to favourable angles of incidence when the laser spot moves away from the cathode edge, however, typical count rates in this region are about 1% of the central region.

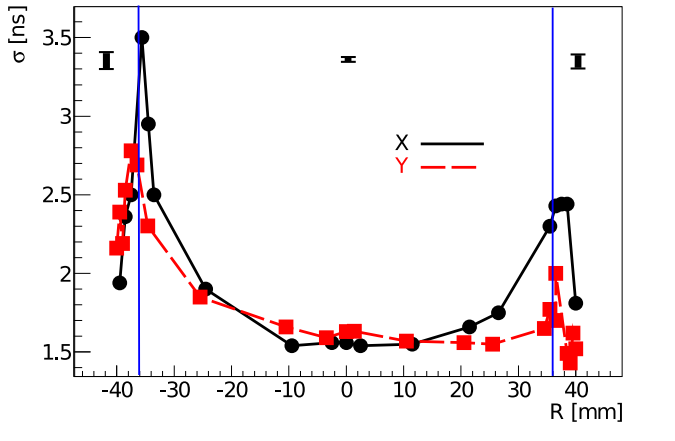

Figure 6: Typical timing characteristics at a gain of 5×10^6. The curves show the transit time spread σ as a function of the position on the PMT entrance window, scanned in the X (black solid line with circle markers) and Y (red (gray) dashed line with rectangular markers) directions, as defined in Fig. 2. The vertical lines mark the effective photo-cathode area. Typical error bars for three different regions are shown on top of the graph.

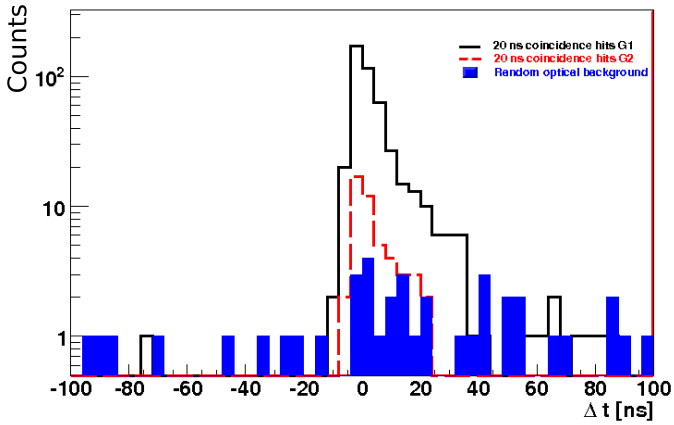

Figure 7: Distributions of time residuals, $\Delta t = t_{reconstructed} - t_{expected}$, of hits from simulated showers in the G1 detector (black solid line) and the G2 detector (red (gray) dashed line) and the random optical background (blue (gray) filled area). For the signal-to-background ratio the time residual interval -10 ns$< \Delta t < 30$ ns was selected.

3.4. Expected performance of the multi-PMT DOM

As mentioned in the introduction, a multi-PMT DOM can provide a better background rejection by requiring local coincidences between neighboring PMTs. Here, we investigate the expected performance of a multi-PMT DOM housing PMTs with the timing characteristics of the D783FL and compare it to a triplet of 10-inch single-PMT OMs as applied in ANTARES. For comparison, we simulated shower events in KM3NeT for two different geometries G1 and G2: G1 has string geometry, consists of 310 strings with 130 m distance between them and 20 floors with 40 m distance between the floors while each floor is equipped with one DOM housing 31 3-inch PMTs [5]. G2 has the same number of strings and floors, but each floor is equipped with a triplet of 10-inch OMs (ANTARES like detector [2]).

We included a typical optical background noise of 60 kHz/PMT for G2, as measured for ANTARES, and, corresponding to the about 12 times smaller cathode area, a background noise of 5.2 kHz/PMT for G1. Furthermore, we chose coincidence hits appearing in a coincidence window of 20 ns for both geometries, as this time window is established as "L1" trigger in ANTARES requiring local coincidences in a single floor. Figure 7 shows the distributions of the difference between the reconstructed and expected time of hits, $\Delta t = t_{reconstructed} - t_{expected}$, for the two shower simulations in the G1 (black solid line) and the G2 (red (gray) dashed line) geometry and for the random optical background (blue (gray) filled area). The power of background rejection in the G2 detector is compared to that in the G1 detector by selecting hits peaking in a time residual interval of -10 ns$< \Delta t < 30$ ns and by calculating the signal to optical-background ratio in the two shower simulations. The results indicate that the G1 detector with the multi-PMT DOMs yields an about 9.4 times higher signal-to-background ratio compared to the G2 detector.

4. Summary

The envisaged multi-PMT DOM of the future deep-sea neutrino telescope KM3NeT puts strong requirements on the PMT design [5]. Several samples of a newly developed 3-inch diameter PMT have been evaluated. Results of the gain linearity, photo-cathode homogeneity, dark-noise rates, after-pulse probabilities, and transit time spread across the PMT surface are satisfactory and according to requirements [9]. The evaluated type of PMT appears to be suitable for the implementation in the multi-PMT DOM of KM3NeT. Accordingly, we have simulated the expected performance of a multi-PMT DOM with the timing performance of the ETEL PMTs and compared it to a detector containing 10-inch single-PMT OMs. The obtained results indicate that the rejection of the random optical background is better by a factor of about 9.4 in the multi-PMT DOM.

This work was supported through the EU-funded FP6 KM3NeT Design Study Contract No. 011937.

5. References

[1] U. Katz, Nucl. Instr. & Meth. A 602 (2009) 40-46.
[2] M. Circella, Nucl. Instr. & Meth. A 602 (2009) 1-6.
[3] A. Capone et al., Nucl. Instr. & Meth. A 602 (2009) 47-53.
[4] P.A. Rapidis, Nucl. Instr. & Meth. A 602 (2009) 54-57.
[5] P. Bagley et al., KM3NeT Technical Design Report, 2011, ISBN 978-90-6488-033-9; http://www.km3net.org/TDR/TDRKM3NeT.pdf.
[6] O. Kavatsyuk, et al., Nucl. Instr. & Meth. A (2011), *in press*, doi:10.1016/j.nima.2011.09.062
[7] Hamamatsu PLP10-40 laser diode head (wavelength 405 nm) with C10196 Controller.
[8] Acqiris DC282 digitizer with 10 bit resolution and 8 GS/s sampling rate.
[9] O. Kalekin. Status of the PMT development for KM3NeT. VLVnT Workshop, Erlangen, Germany, 12-14 Oct 2011.

Table 2: Measured performance parameters of D783FL PMTs

PMT serial number	Nominal voltage [V] (Gain $\approx 5 \times 10^6$)	supply voltage [V]	Gain @ supply voltage	P/V (no laser)	P/V (laser)	σ (TTS) at center [ns]	Dark rate [kHz]	Afterpulses (400 ns window) [%]
SN172	970	970	5.3×10^6	2.0	2.5	1.7	0.9	0.7
		700	5.4×10^5		2.8	2.5	0.9	
SN174	1170	1170	6.1×10^6	2.9	3.3	1.4	1.1	3.2
		850	5.7×10^5		2.8	1.9	1.1	
SN175	985	985	6.4×10^6	2.8	3.6	1.7	1.7	6.2
		750	8×10^5		2.5	2.2	1.0	
SN185	1310	1310	6.3×10^6	2.5	3.2	1.3	1.3	3.0
		900	4.8×10^5		3.1	1.8	0.7	
SN189	1230	1230	6.6×10^6	2.8	3.8	1.4	1.1	6.0
		900	5.7×10^5		2.3	1.8	0.8	